Hindawi
Mathematical Problems in Engineering
Volume 2019, Article ID 4957259, 16 pages
https://doi.org/10.1155/2019/4957259

Research Article

Extension of Leader-Follower Behaviours for Wheeled Mobile Robots in Multirobot Coordination

P. Paniagua-Contro,[1] E. G. Hernandez-Martinez,[1] O. González-Medina,[2] J. González-Sierra,[3] J. J. Flores-Godoy,[4] E. D. Ferreira-Vazquez,[5] and G. Fernandez-Anaya[6]

[1]*Engineering Department, Universidad Iberoamericana, 01219 Mexico City, Mexico*
[2]*Tecnológico Nacional de México/I.T. La Laguna, 27000 Torreón, Mexico*
[3]*CONACyT-Tecnológico Nacional de México/I.T. La Laguna, 27000 Torreón, Mexico*
[4]*Mathematics Department, Universidad Católica del Uruguay, 11600 Montevideo, Uruguay*
[5]*Electrical Engineering Department, Universidad Católica del Uruguay, 11600 Montevideo, Uruguay*
[6]*Physics and Mathematics Department, Universidad Iberoamericana, 01219 Mexico City, Mexico*

Correspondence should be addressed to J. J. Flores-Godoy; jose.flores@ucu.edu.uy

Received 14 September 2018; Revised 14 December 2018; Accepted 27 January 2019; Published 2 April 2019

Academic Editor: Xiangyu Meng

This paper presents the extension of leader-follower behaviours, for the case of a combined set of kinematic models of omnidirectional and differential-drive wheeled mobile robots. The control strategies are based on the decentralized measurements of distance and heading angles. Combining the kinematic models, the control strategies produce the standard and new mechanical behaviours related to rigid body or n-trailer approaches. The analysis is given in pairs of robots and extended to the case of multiple robots with a directed tree-shaped communication topology. Combining these behaviours, it is possible to make platoons of robots, as obtained from cluster space or virtual structure approaches, but now defined by local measurements and communication of robots. Numerical simulations and real-time experiments show the performance of the approach and the possibilities to be applied in multirobot tasks.

1. Introduction

The coordination of multiple mobile robots has found a wide field of applications in the industry, surveillance, home services, logistics, among others [1]. It extends the classical problems of point convergence and trajectory tracking of a unique mobile robot to the case of collective behaviours like the convergence to formation patterns, formation tracking, dispersion, containment, interrobot collision avoidance, etc. The design of formation patterns has been studied in structured and behavioural approaches and the approaches inspired on multicellular mechanism, according to [2]. The possible interactions between robots are represented by a communication topology which is predefined by the designer or by the proximity of the robots. The control laws require the feedback of the global position of the robots or their relative displacements, distances, and angles according to the sensor installed in the workspace or locally in the robots [3–5].

The problem of formation tracking requires the simultaneous convergence of the robots to a formation pattern and a target or trajectory. The most basic scheme of multirobot formation tracking is the case of two robots, where a leader follows the trajectory, and the follower agent must satisfy a relative posture with respect to the leader. In a decentralized manner, the control strategy depends on the local measurements of distance and heading or absolute angles. A pioneer work can be found in [6], where a follower robot is formed with respect to one or two leaders. In [7] the desired position of the follower is given by a virtual unicycle robot. The estimation of the posture of a single leader is given in

[8]. The leader-follower behaviour designed for two robots is extended to multiple robots in [9], to achieve directed tree-shaped configurations. All the previous works analyse the local convergence only and infer the global convergence in the settling times, but they avoid formal proofs about the stability of the whole system, with an arbitrary number of robots.

On the other hand, the study of the global convergence of distance-based formation control has been studied in the context of formation graphs [10]. Such is the case of [11] using distances and PI controllers, time-varying formation in [12], the addition of area constraints in [13, 14] for triangle formations, or the use of Model Predictive Control based on neural-dynamic optimization in [15], among others. In the context of formation graphs, the extension of the leader-follower formations is falling in the case of directed graphs with a unique leader node, as presented in [16]. A unified, distributed formation control scheme that accommodates an arbitrary number of group leaders and an arbitrary information flow among vehicles is presented in [17]. The architecture requires the local information exchange among neighbours only. An extended consensus algorithm is applied on the group level to estimate the time-varying group trajectory information. Using the estimated group trajectory information, a consensus-based distributed formation control strategy is then applied for the vehicle level control. In [18], a merging strategy for cooperative vehicles is addressed. Each vehicle possesses a tracking controller considering both tracking and coupling error signals, where all vehicles in the group know their positions. The trajectories of the cooperative vehicles are planned, to guarantee that each vehicle keeps a certain distance from the rest of the vehicles, and are designed by using the virtual structure approach. The merging strategy is validated in an experimental platform consisting of a group of nonholonomic mobile vehicles representing a basic bicycle model for cars with a zero vehicle length. Using the Lyapunov theory, it is showed that the strategy is global asymptotically stable for the group. In [19], the authors propose a hierarchical control scheme based on the definition of multirobot task functions. The scheme faces the following tasks for controlling the behaviour of multirobot systems: (1) the time parametrization of tasks and (2) smooth task transitions. It is demonstrated that both aspects can be solved by means of terminal attractors. Also the robustness and versatility of the proposed scheme with global tasks in simulation and one experiment considering local tasks with a set of wheeled robots are verified.

For the case of wheeled mobile robots moving in the plane, the kinematic and dynamic models commonly used in industrial and service applications are the differential-drive mobile robots and the omnidirectional (with mecanum and omnidirectional wheels) robots [20]. Example of implementation of these wheeled mobile robots is found in [21], for the case of real object transportation. Also, the work in [22] addresses a tractor convoy used in agriculture to move loads and following waypoints. Finally, in [23] the object transportation in an industrial area collaborating with unmanned aerial robots is presented.

Experimental work for the previous wheeled mobile robots, mostly for the case of differential-drive robots, has been presented in [24] considering the dynamics of their on-board leader trackers. The on-board cameras perspective and calibration are studied in [25], and the bounded single-view distance estimation of cameras is presented in [26]. Control laws to maintain the visibility of the leader in the presence of obstacles are given in [27]. Nonlinear estimators for aircrafts using a seeker sensor are presented in [9]. Finally, the possible reassignation of the leader based on an affection fuzzy measurement is proposed by [28].

For the extension of the leader-follower strategies, to the case of collaborative object transportation or target tracking, some global interrobot structures are imposed for the robots. The first case is the generation of virtual trajectories or navigation functions for the followers, moving with respect to the leader, as in [29]. The second strategy is the creation of virtual robots or targets placed on the center of circles to generate polygons-shaped formations for the followers [30]. This idea is extended for column subgroups of robots with center of rotation in a hierarchical setup in [31]. The third concept is the definition of virtual structures, where the desired position of the robots is defined in a structure which is moved along a trajectory. Therefore, the control for each robot is designed to converge to its global position in the structure. Some examples are given in [32], with a human operator moving the virtual structure, [33] for the case of intelligent vehicles, [34] using the dynamical model of the virtual structure and [35] for some infinitesimally and minimally rigid frameworks. A special virtual structure is the so-called V-shape formation, where a leader is placed in a root node, and lines of followers are placed with respect to a global angle related to the root node [36]. Finally, the concept of imposing a moving global structure is also referred to as the cluster space specifications in [37, 38], which imposes the dynamics of an object to be transported and specifies the positions of the robots under these object. Note that all the previous strategies impose for the robots the knowledge of global coordinates, velocities, and other dynamical references to be measured.

Inspired by [6] and our previous work of distance-based formation control given in [4, 39], this paper contributes to the context of the leader-follower formation of wheeled mobile robots. The originality and contributions are summarized in the next points:

(i) This paper addresses the leader-follower behaviour applied to the kinematic model of the omnidirectional robot. A differential-drive model can be obtained by cancelling the lateral linear velocity. Therefore, the approach becomes heterogeneous combining the most common wheeled vehicles used in the practice.

(ii) Four basic leader-follower control laws are defined due the combination of the omnidirectional and differential-drive robots. The local convergence is proved. It extends the results of [6] and the case presented in [39], limited only to two omnidirectional robots. The control laws are designed to be decentralized using the measurement of distance

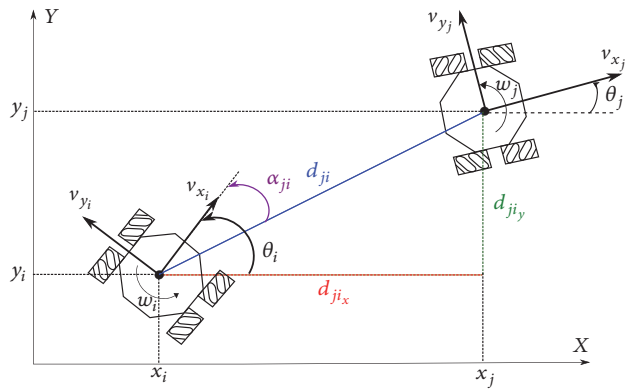

FIGURE 1: Schematic diagram for the leader-follower approach.

and the heading angle with respect to the leader, avoiding the use of global references as mentioned before. Furthermore, they require the velocities from the leader which can be obtained from a wireless communication.

(iii) It is proved that the robots converge to the classical rigid motion behaviour and the standard n-trailer. Also, by the heterogeneous concept of the system, we introduce a new mechanical device called omnitrailer. As far as we know, the demonstration of these local behaviours in the settling time has not been reported in the literature.

(iv) It is shown that the extension of the four control laws can generate formation tracking, useful for object transportation or collaborative tasks if the robots satisfy a directed tree-shaped topology. By numerical simulation, convoy-like formation of rigid platoons of robots can be achieved. Thus, it is possible to generate complex behaviours like virtual structures or cluster space specifications, avoiding the information of a global reference framework.

(v) Finally, the control approach is evaluated by a numerical simulation and experimental work using, in a first step, a motion capture system.

The paper is organized as follows. The problem definition is given in Section 2. Some preliminaries are given in Section 3, while the main results about the control strategies are defined and analysed in Section 4. The extension to groups of mobile robots in directed tree-shaped formation tracking is given by numerical simulations in Section 5. Real-time experiments are presented in Section 6. Finally, some conclusion remarks and future work are presented in Section 7.

2. Problem Definition

Let $N = \{R_1, \ldots, R_n\}$ be a group of n omnidirectional robots (see Figure 1). The kinematic model of the omnidirectional robots is given by

$$\dot{\boldsymbol{\xi}}_i = R(\theta_i)\,\mathbf{u}_i, \quad i = 1, \ldots, n, \tag{1}$$

where $R(\theta_i)$ is the rotation matrix defined by

$$R(\theta_i) = \begin{bmatrix} \cos\theta_i & -\sin\theta_i & 0 \\ \sin\theta_i & \cos\theta_i & 0 \\ 0 & 0 & 1 \end{bmatrix}, \tag{2}$$

$\boldsymbol{\xi}_i = [x_i \;\; y_i \;\; \theta_i]^\top \in \mathbb{R}^3$ is the state vector with $x_i, y_i \in \mathbb{R}$ as the position in the plane of the i–th agent, $\theta_i \in \mathbb{R}$ is the orientation with respect to the horizontal axis, $\mathbf{u}_i = [v_{x_i} \;\; v_{y_i} \;\; w_i]^\top$ is the control input vector with $v_{x_i} \in \mathbb{R}$ as the longitudinal velocity, $v_{y_i} \in \mathbb{R}$ is the lateral velocity, and $w_i \in \mathbb{R}$ is the angular velocity.

Remark 1. It is worth mentioning that if the lateral velocity $v_{y_i} = 0$, for all time in (1), one can obtain the kinematic model of a differential-drive robot given by

$$\dot{\boldsymbol{\xi}}_i = \begin{bmatrix} \cos\theta_i & 0 \\ \sin\theta_i & 0 \\ 0 & 1 \end{bmatrix} \begin{bmatrix} v_{x_i} \\ w_i \end{bmatrix} \quad i = 1, \ldots, n. \tag{3}$$

It is clear that a physical differential-drive robot and any kind of physical omnidirectional robot, suppressing its lateral velocity v_{y_i}, can perform the motion given in (3). In the latter case, the same robot can be switched between (1) and (3), as shown below.

The focus of this article is to extend the results presented in [39] to a group of n agents. In this, a dynamic model, of a multiagent heterogeneous system composed of omnidirectional and differential-drive robots, based on the distance and angle between a pair of robots will be developed, *i.e.*,

$$\dot{\boldsymbol{\eta}}_{ji} = \left[\dot{d}_{ji} \;\; \dot{\alpha}_{ji} \;\; \dot{e}_{\theta_{ji}}\right]^\top = f\left(d_{ji}, \alpha_{ji}, e_{\theta_{ji}}, \mathbf{u}_j, \mathbf{u}_i\right), \tag{4}$$

where $d_{ji} \in \mathbb{R}_+$ is the distance measured from the geometrical center of agent R_j to the geometrical center of the agent R_i, with $\mathbb{R}_+$ as the set of all positive real numbers, d_{ji_x} and $d_{ji_y} \in \mathbb{R}_+$ are the components of the distance vector $\boldsymbol{d}_{ji}$ with respect to a global frame, $\alpha_{ji} \in \mathbb{R}$ is the formation angle measured from the distance vector $\boldsymbol{d}_{ji}$ to a local frame attached to the agent R_i, and $\mathbf{u}_j$ and $\mathbf{u}_i$ are the vector control inputs, for the leader and follower, respectively, while $e_{\theta_{ji}}$ is the orientation error angle between the leader and the follower. Note that (4) is a general representation of the model and, as it will be shown, particular cases will be defined later on. Once the model is obtained, a control strategy is designed, such that

(i) $\lim_{t\to\infty}(d_{ji} - d^*_{ji}) = 0$, where d^*_{ji} is the desired distance;

(ii) $\lim_{t\to\infty}(\alpha_{ji} - \alpha^*_{ji}) = 0$, where α^*_{ji} is the desired angle.

This means that R_i will keep a distance and heading orientation with respect to R_j. Depending on the kinematics model of both robots (omnidirectional or differential-drive), some control laws, developed in Section 4, will generate, in the steady state, different mechanical structures.

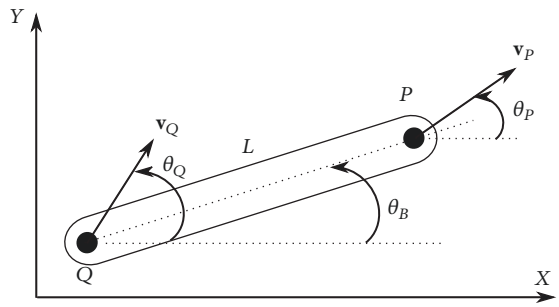

Figure 2: Motion equation of two points of a rigid body.

3. Preliminaries

A reminder of the rigid motion equation, the kinematic model of the standard 1-trailer, and a new rigid structure will be given in this section. This will help us to validate the main results of this article.

3.1. Rigid Body Motion Equation. The velocity relationship between any two points of a rigid body (see Figure 2) can be expressed by the rigid body motion equation [20] given as

$$\mathbf{v}_Q = \mathbf{v}_P + \boldsymbol{w}_B \times \boldsymbol{r}_{PQ}, \tag{5}$$

where $\mathbf{v}_P$ and $\mathbf{v}_Q$ are the velocities of the points P and Q, respectively, $\boldsymbol{w}_B$ is the angular velocity of the rigid body, $\boldsymbol{r}_{PQ}$ is the position vector from point P to point Q, θ_Q and θ_P are the orientations of the velocities of points Q and P, respectively, and L is the distance between P and Q. Considering a two-dimensional space, therefore, the rigid body motion equation (5) has to satisfy the following expressions:

$$\left|\mathbf{v}_Q\right| \cos\theta_Q = \left|\mathbf{v}_P\right| \cos\theta_P + L\dot{\theta}_B \sin\theta_B, \tag{6a}$$

$$\left|\mathbf{v}_Q\right| \sin\theta_Q = \left|\mathbf{v}_P\right| \sin\theta_Q - L\dot{\theta}_B \cos\theta_B. \tag{6b}$$

3.2. Kinematic Model of a Standard 1-Trailer. From Figure 1, suppose that $v_{y_i} = v_{y_j} = 0$ and $\alpha_{ji} = 0$. This means that both agents are differential-drive robots. Consider that the agents are linked through mechanical joints, obtaining the scheme for the standard 1–trailer with kinematic model given by (Rouchon et al. [40]; Orosco-Guerrero et al. [41]; Bushnell et al. [42])

$$\dot{x}_j = v_{x_j} \cos\theta_j, \tag{7a}$$

$$\dot{y}_j = v_{x_j} \sin\theta_j, \tag{7b}$$

$$\dot{\theta}_j = w_j, \tag{7c}$$

$$\dot{\theta}_i = v_{x_j} \frac{\sin\left(\theta_j - \theta_i\right)}{d_{ji}}, \tag{7d}$$

where $\begin{bmatrix} x_j & y_j \end{bmatrix}^\top \in \mathbb{R}^2$ are the coordinates of the midpoint of the wheels axis of the tractor and θ_j and θ_i are the orientation of the tractor and trailer, respectively, with respect to the horizontal axis, while v_{x_j} and w_j are the control inputs corresponding to the linear and angular velocities of the tractor, respectively. Therefore, we have the following evident result.

Lemma 2. *The linear velocity of the trailer v_{x_i} depends on the linear velocity of the tractor v_{x_j} and the orientations θ_j and θ_i and is given by*

$$v_{x_i} = v_{x_j} \cos\left(\theta_j - \theta_i\right). \tag{8}$$

3.3. Omnitrailer. Due to the heterogeneous structure of the trailer system, it is possible to have an omnidirectional robot as a tractor (leader robot) and, therefore, Lemma 2 can be extended. From Figure 1 suppose that $v_{y_i} = 0$; hence, R_i is a differential-drive robot, which is pulled by an omnidirectional robot and they are linked by a rigid bar of length d_{ji}. In consequence, we have the following evident Lemma.

Lemma 3. *The linear velocity v_{x_i} and the angular velocity w_i of the differential-drive robot depend on the velocities v_{x_j} and v_{y_j} and the angles θ_j and θ_i and is given by*

$$v_{x_i} = v_{x_j} \cos\left(\theta_j - \theta_i\right) - v_{y_j} \sin\left(\theta_j - \theta_i\right), \tag{9a}$$

$$\dot{\theta}_i = \frac{1}{d_{ji}} \left[v_{x_j} \sin\left(\theta_j - \theta_i\right) + v_{y_j} \cos\left(\theta_j - \theta_i\right) \right]. \tag{9b}$$

4. Control Strategy

In this section, the dynamic model, based on distance and orientation, referred in (4), is developed considering, in a first step, a group of n omnidirectional robots. Then, by cancelling some velocities it is possible to obtain a dynamic model for a heterogeneous system, composed by omnidirectional and differential-drive robots. In this context, four different dynamic models are developed.

$\mathcal{O} - \mathcal{O}$ Leader-Follower Scheme. Both agents R_i and R_j are omnidirectional robots.

$\mathcal{U} - \mathcal{O}$ Leader-Follower Scheme. Agent R_j is a differential-drive robot and R_i is an omnidirectional robot.

$\mathcal{U} - \mathcal{U}$ Leader-Follower Scheme. Both agents R_i and R_j are differential-drive robots.

$\mathcal{O} - \mathcal{U}$ Leader-Follower Scheme. Agent R_j is an omnidirectional robot and agent R_i is a differential-drive robot.

In a second step, four control strategies are designed, by means of linearizing techniques, to achieve rigid platoons of robots. Finally, a global control strategy is developed taking into account a group of n mobile robots.

4.1. $\mathcal{O}$-$\mathcal{O}$ Leader-Follower Scheme. Based on Figure 1, the distance d_{ji} and the angle α_{ji}, with $i = 1,\ldots,n-1$ and $j = 1,\ldots,n$, $j \neq i$, are given by

$$d_{ji} = \sqrt{\left(x_j - x_i\right)^2 + \left(y_j - y_i\right)^2} = \sqrt{d_{ji_x}^2 + d_{ji_y}^2}, \tag{10a}$$

$$\alpha_{ji} = \theta_i - \tan^{-1}\left(\frac{y_j - y_i}{x_j - x_i}\right), \tag{10b}$$

where $d_{ji_x} = x_j - x_i$ and $d_{ji_y} = y_j - y_i$. The time-derivative of (10a) and (10b) is given by

$$\dot{d}_{ji} = \frac{d_{ji_x}\dot{d}_{ji_x} + d_{ji_y}\dot{d}_{ji_y}}{d_{ji}}, \tag{11a}$$

$$\dot{\alpha}_{ji} = \dot{\theta}_i - \frac{d_{ji_x}\dot{d}_{ji_y} - d_{ji_y}\dot{d}_{ji_x}}{d_{ji}^2}, \tag{11b}$$

with

$$\dot{d}_{ji_x} = v_{x_j}\cos\theta_j - v_{y_j}\sin\theta_j - v_{x_i}\cos\theta_i + v_{y_i}\sin\theta_i, \tag{12a}$$

$$\dot{d}_{ji_y} = v_{x_j}\sin\theta_j + v_{y_j}\cos\theta_j - v_{x_i}\sin\theta_i - v_{y_i}\cos\theta_i. \tag{12b}$$

Substituting (12a) and (12b) into (11a) and (11b) and considering that $d_{ji_x} = d_{ji}\cos(\theta_i - \alpha_{ji})$ and $d_{ji_y} = d_{ji}\sin(\theta_i - \alpha_{ji})$, therefore (11a) and (11b) can be expressed as

$$\dot{\boldsymbol{\eta}}_{ji} = f_{\eta_{ji}}\left(\boldsymbol{\eta}_{ji}\right)\mathbf{u}_j + g_{\eta_{ji}}\left(\boldsymbol{\eta}_{ji}\right)\mathbf{u}_i, \quad i \neq j, \tag{13}$$

with

$$f_{\eta_{ji}} = \begin{bmatrix} \cos\left(e_{\theta_{ji}} + \alpha_{ji}\right) & -\sin\left(e_{\theta_{ji}} + \alpha_{ji}\right) & 0 \\ -\dfrac{\sin\left(e_{\theta_{ji}} + \alpha_{ji}\right)}{d_{ji}} & -\dfrac{\cos\left(e_{\theta_{ji}} + \alpha_{ji}\right)}{d_{ji}} & 0 \\ 0 & 0 & 1 \end{bmatrix}, \tag{14a}$$

$$g_{\eta_{ji}} = \begin{bmatrix} -\cos\alpha_{ji} & \sin\alpha_{ji} & 0 \\ \dfrac{\sin\alpha_{ji}}{d_{ji}} & \dfrac{\cos\alpha_{ji}}{d_{ji}} & 1 \\ 0 & 0 & -1 \end{bmatrix}, \tag{14b}$$

where $\boldsymbol{\eta}_{ji} = \begin{bmatrix} d_{ji} & \alpha_{ji} & e_{\theta_{ji}} \end{bmatrix}^\top$ is the state vector and $e_{\theta_{ji}} = \theta_j - \theta_i$. Since both agents are omnidirectional mobile robots, therefore, $\mathbf{u}_j = \begin{bmatrix} v_{x_j} & v_{y_j} & w_j \end{bmatrix}^\top$ and $\mathbf{u}_i = \begin{bmatrix} v_{x_i} & v_{y_i} & w_i \end{bmatrix}^\top$. Note that (13) is a special case of the general model given in (4).

The static state feedback control, for system (13), is given as

$$\mathbf{u}_i = g_{\eta_{ji}}^{-1}\left(-f_{\eta_{ji}}\mathbf{u}_j + \mathbf{p}_{ji}\right), \tag{15}$$

where $\mathbf{p}_{ji}$ is defined by

$$\mathbf{p}_{ji} = \begin{bmatrix} \dot{d}_{ji}^* - k_d e_{d_{ji}} \\ \dot{\alpha}_{ji}^* - k_\alpha e_{\alpha_{ji}} \\ -k_\theta e_{\theta_{ji}} \end{bmatrix}, \tag{16}$$

with k_d, k_α, and k_θ being positive design gains, and $e_{d_{ji}} = d_{ji} - d_{ji}^*$ and $e_{\alpha_{ji}} = \alpha_{ji} - \alpha_{ji}^*$ are the distance error and the formation orientation error, respectively.

Theorem 4. *Consider system (13) in closed-loop with (15) and (16); therefore, the error coordinates $e_{d_{ji}}$, $e_{\alpha_{ji}}$, and $e_{\theta_{ji}}$ tend to zero, i.e., $\lim_{t\to\infty} e_{d_{ji}} = \lim_{t\to\infty} e_{\theta_{ji}} = \lim_{t\to\infty} e_{\alpha_{ji}} = 0$.*

Proof. The dynamics of the error coordinates are given by

$$\dot{\mathbf{e}}_{ji} = \dot{\boldsymbol{\eta}}_{ji} - \dot{\boldsymbol{\eta}}_{ji}^*, \tag{17}$$

where $\mathbf{e}_{ji} = \begin{bmatrix} e_{d_{ji}} & e_{\alpha_{ji}} & e_{\theta_{ji}} \end{bmatrix}^\top$, $\boldsymbol{\eta}_{ji}^* = \begin{bmatrix} d_{ji}^* & \alpha_{ji}^* & 0 \end{bmatrix}^\top$. Substituting (13), (15), and (16) into (17), then, one obtains

$$\dot{\mathbf{e}}_{ji} = -K_{ji}\mathbf{e}_{ji}, \tag{18}$$

where $K_{ji} = \operatorname{diag}\{k_d, k_\alpha, k_\theta\}$ is a diagonal matrix. Note that $-K_{ji}$ is a Hurwitz matrix if k_d, k_α, and $k_\theta > 0$; hence, $\lim_{t\to\infty} e_{d_{ji}} = \lim_{t\to\infty} e_{\theta_{ji}} = \lim_{t\to\infty} e_{\alpha_{ji}} = 0$ and the agent R_i keeps a distance and orientation with respect to the agent R_j. □

Remark 5. Note that the $\mathcal{O}$-$\mathcal{O}$ Scheme was studied in [39] considering only two omnidirectional robots. However, part of this work extends the results for a group of n omnidirectional robots.

4.2. $\mathcal{U}$-$\mathcal{O}$ Leader-Follower Scheme

Proposition 6. *Let R_j be a differential-drive robot and R_i be an omnidirectional robot. In this sense, $v_{y_j} = 0$ and the system (13) is rewritten as*

$$\dot{\overline{\boldsymbol{\eta}}}_{ji} = \overline{f}_{\eta_{ji}}\left(\boldsymbol{\eta}_{ji}\right)\overline{\mathbf{u}}_j + \overline{g}_{\eta_{ji}}\left(\boldsymbol{\eta}_{ji}\right)\overline{\mathbf{u}}_i, \quad i \neq j, \tag{19}$$

where $\overline{g}_{\eta_{ji}} = g_{\eta_{ji}}$, as in (14b), $\overline{\mathbf{u}}_j = \begin{bmatrix} v_{x_j} & w_j \end{bmatrix}^\top$, $\overline{\mathbf{u}}_i = \begin{bmatrix} v_{x_i} & v_{y_i} & w_i \end{bmatrix}^\top$, and

$$\overline{f}_{\eta_{ji}} = \begin{bmatrix} \cos\left(e_{\theta_{ji}} + \alpha_{ji}\right) & 0 \\ -\dfrac{\sin\left(e_{\theta_{ji}} + \alpha_{ji}\right)}{d_{ji}} & 0 \\ 0 & 1 \end{bmatrix}. \tag{20}$$

The static state linearizing feedback control law is given by

$$\overline{\mathbf{u}}_i = \overline{g}_{\eta_{ji}}^{-1}\left(-\overline{f}_{\eta_{ji}}\overline{\mathbf{u}}_j + \mathbf{p}_{ji}\right), \tag{21}$$

with the same auxiliary control given in (16).

Remark 7. Note that in the $\mathcal{O}-\mathcal{O}$ and $\mathcal{U}-\mathcal{O}$ leader-follower scheme the determinant of the matrices $g_{\eta_{ji}}$ and $\overline{g}_{\eta_{ji}}$ is the same, *i.e.*, $\det(g_{\eta_{ji}}) = \det(\overline{g}_{\eta_{ji}}) = 1/d_{ji}$. Since the parameter d_{ji} is the distance from agent R_j to R_i, therefore $d_{ji} > 0$ and matrices $g_{\eta_{ji}}$ and $\overline{g}_{\eta_{ji}}$ will be always invertible. Furthermore, if the parameter d_{ji} is close to zero, it implies that the agents are very close to each other, which is not feasible, due to the dimensional restrictions of the robots. Hence, in this scheme, the control performance is not constrained.

4.3. $\mathcal{U}$-$\mathcal{U}$ Leader-Follower Scheme

Proposition 8. *Let agents R_i and R_j be differential-drive robots, hence, $v_{y_i} = v_{y_j} = 0$, and functions $f_{\eta_{ji}}$ and $g_{\eta_{ji}}$, of (14a) and (14b), are rewritten as*

$$\widehat{f}_{\eta_{ji}} = \begin{bmatrix} \cos\left(e_{\theta_{ji}} + \alpha_{ji}\right) & 0 \\ -\dfrac{\sin\left(e_{\theta_{ji}} + \alpha_{ji}\right)}{d_{ji}} & 0 \\ 0 & 1 \end{bmatrix},$$
$$\widehat{g}_{\eta_{ji}} = \begin{bmatrix} -\cos\alpha_{ji} & 0 \\ \dfrac{\sin\alpha_{ji}}{d_{ji}} & 1 \\ 0 & -1 \end{bmatrix}. \tag{22}$$

Taking into account the output function $\widehat{\mathbf{h}}_{ji} = \begin{bmatrix} d_{ji} & \alpha_{ji} \end{bmatrix}^\top$, the following system is obtained:

$$\dot{\widehat{\mathbf{h}}}_{ji} = \widehat{f}_{h_{ji}}\left(\widehat{\mathbf{h}}_{ji}, e_{\theta_{ji}}\right)\widehat{\mathbf{u}}_j + \widehat{g}_{h_{ji}}\left(\widehat{\mathbf{h}}_{ji}\right)\widehat{\mathbf{u}}_i, \tag{23}$$

with $\widehat{\mathbf{u}}_j = \begin{bmatrix} v_{x_j} & w_j \end{bmatrix}^\top$, $\widehat{\mathbf{u}}_i = \begin{bmatrix} v_{x_i} & w_i \end{bmatrix}^\top$ and

$$\widehat{f}_{h_{ji}} = \begin{bmatrix} \cos\left(e_{\theta_{ji}} + \alpha_{ji}\right) & 0 \\ -\dfrac{\sin\left(e_{\theta_{ji}} + \alpha_{ji}\right)}{d_{ji}} & 0 \end{bmatrix},$$
$$\widehat{g}_{h_{ji}} = \begin{bmatrix} -\cos\alpha_{ji} & 0 \\ \dfrac{\sin\alpha_{ji}}{d_{ji}} & 1 \end{bmatrix}. \tag{24}$$

Since $\det(\widehat{g}_{h_{ji}}) = -\cos\alpha_{ji}$, with $\alpha_{ji} \neq \pm\pi/2$, then, it is possible to define a linearizing feedback control law given by

$$\widehat{\mathbf{u}}_i = \widehat{g}_{h_{ji}}^{-1}\left(-\widehat{f}_{h_{ji}}\widehat{\mathbf{u}}_j + \widehat{\mathbf{p}}_{ji}\right), \tag{25a}$$

$$\widehat{\mathbf{p}}_{ji} = \begin{bmatrix} \dot{d}_{ji}^* - k_d e_{d_{ji}} \\ \dot{\alpha}_{ji}^* - k_\alpha e_{\alpha_{ji}}, \end{bmatrix}, \tag{25b}$$

where $e_{d_{ji}} = d_{ji} - d_{ji}^*$, $e_{\alpha_{ji}} = \alpha_{ji} - \alpha_{ji}^*$ are the distance error and the formation orientation error, respectively, while k_d and k_α are positive design gains. Due to the simplified model obtained for the differential-drive robots, the control law (25a) and (25b) is related only for two control variables.

4.4. $\mathcal{O}$-$\mathcal{U}$ Leader-Follower Scheme

Proposition 9. *Let R_j be an omnidirectional robot and R_i be a differential-drive robot. In this context, $v_{y_i} = 0$ and the functions $\widetilde{f}_{\eta_{ji}} = f_{\eta_{ji}}$, given in (14a), and $\widetilde{g}_{\eta_{ji}} = \widehat{g}_{\eta_{ji}}$, given in (22). Taking into account the output function $\widetilde{\mathbf{h}}_{ji} = \begin{bmatrix} d_{ji} & \alpha_{ji} \end{bmatrix}^\top$, the following system is obtained:*

$$\dot{\widetilde{\mathbf{h}}}_{ji} = \widetilde{f}_{h_{ji}}\left(\widetilde{\mathbf{h}}_{ji}, e_{\theta_{ji}}\right)\widetilde{\mathbf{u}}_j + \widetilde{g}_{h_{ji}}\left(\widetilde{\mathbf{h}}_{ji}\right)\widetilde{\mathbf{u}}_i, \tag{26}$$

with $\widetilde{\mathbf{u}}_j = \begin{bmatrix} v_{x_j} & v_{y_j} & w_j \end{bmatrix}^\top$, $\widetilde{\mathbf{u}}_i = \begin{bmatrix} v_{x_i} & w_i \end{bmatrix}^\top$ and

$$\widetilde{f}_{h_{ji}} = \begin{bmatrix} \cos\left(e_{\theta_{ji}} + \alpha_{ji}\right) & -\sin\left(e_{\theta_{ji}} + \alpha_{ji}\right) & 0 \\ -\dfrac{\sin\left(e_{\theta_{ji}} + \alpha_{ji}\right)}{d_{ji}} & -\dfrac{\cos\left(e_{\theta_{ji}} + \alpha_{ji}\right)}{d_{ji}} & 0 \end{bmatrix},$$
$$\widetilde{g}_{h_{ji}} = \begin{bmatrix} -\cos\alpha_{ji} & 0 \\ \dfrac{\sin\alpha_{ji}}{d_{ji}} & 1 \end{bmatrix}. \tag{27}$$

Since $\det(\widetilde{g}_{h_{ji}}) = -\cos\alpha_{ji}$, with $\alpha_{ji} \neq \pm\pi/2$, then, it is possible to define a linearizing feedback control law given by

$$\widetilde{\mathbf{u}}_i = \widetilde{g}_{h_{ji}}^{-1}\left(-\widetilde{f}_{h_{ji}}\widetilde{\mathbf{u}}_j + \widetilde{\mathbf{p}}_{ji}\right), \tag{28}$$

with $\widetilde{\mathbf{p}}_{ji} = \widehat{\mathbf{p}}_{ji}$.

Remark 10. Recall that the angle α_{ji} is the angle measured from the distance vector $\boldsymbol{d}_{ji}$ to a local frame attached to the agent R_i. In this sense, an angle $\alpha_{ji} = \pm\pi/2$ means that the component of the velocity perpendicular to the wheels of the differential-drive mobile robots is aligned to the distance vector $\boldsymbol{d}_{ji}$, and, due to the nonholonomic restriction of this kind of vehicles, given by $\dot{x}_i \sin\theta_i - \dot{y}_i \cos\theta_i = 0$, then the motion, perpendicular to the linear velocity, is zero. Therefore, the restriction of $\alpha_{ji} \neq \pm\pi/2$ implies the nonholonomic restriction of the differential-drive mobile robots.

Remark 11. By a similar procedure to Theorem 4, it can be shown that from system (19) with control (21) the error coordinates will converge to zero, *i.e.*, $\lim_{t\longrightarrow\infty} e_{d_{ji}} = \lim_{t\longrightarrow\infty} e_{\theta_{ji}} = \lim_{t\longrightarrow\infty} e_{\alpha_{ji}} = 0$. Furthermore, from system (23) with control (25a) and (25b) and system (26) with control (28), the errors $e_{d_{ji}}$ and $e_{\alpha_{ji}}$ will converge to zero, *i.e.*, $\lim_{t\longrightarrow\infty} e_{d_{ji}} \lim_{t\longrightarrow\infty} e_{\alpha_{ji}} = 0$.

4.5. Global Control Strategy. This subsection states a relevant contribution of the article. Specifically, a global control strategy is developed to ensure that a group of agents, composed by omnidirectional and differential-drive mobile robots, converge to a desired distance and formation angle.

Recall that N is a group of n agents where R_n is the leader, represented by an omnidirectional mobile robot, while the rest are the followers that could be omnidirectional or differential-drive mobile robots, and suppose that $j > i$, then, the dynamic model of the group can be represented by

$$\dot{\boldsymbol{\zeta}} = \mathscr{L}\mathbb{U}, \tag{29}$$

where $\boldsymbol{\zeta}$ is the state vector containing the distances, formation angles, and orientations with respect a pair of agents, $\mathbb{U}$ is the control input, and $\mathscr{L}$ is an upper triangular block matrix.

Remark 12. Without loss of generality, consider that the agents are under the well-known directed open-chain formation, and let us assume that the agents are ordered as follows:

$N = \{\mathcal{O}, \mathcal{U}, \mathcal{U}, \mathcal{O}, \ldots, \mathcal{O}, \mathcal{U}, \mathcal{U}, \mathcal{O}, \mathcal{O}\}$, then, the state vector $\boldsymbol{\zeta}$, the control input $\mathbb{U}$, and the matrix $\mathscr{L}$ are given as follows:

$$\boldsymbol{\zeta} = \begin{bmatrix} \overline{\boldsymbol{\eta}}_{21} \\ \widehat{\mathbf{h}}_{32} \\ \widetilde{\mathbf{h}}_{43} \\ \boldsymbol{\eta}_{54} \\ \vdots \\ \overline{\boldsymbol{\eta}}_{(n-3)(n-4)} \\ \widehat{\mathbf{h}}_{(n-2)(n-3)} \\ \widetilde{\mathbf{h}}_{(n-1)(n-2)} \\ \boldsymbol{\eta}_{n(n-1)} \\ \boldsymbol{\xi}_n \end{bmatrix}, \tag{30}$$

$$\mathbb{U} = \begin{bmatrix} \overline{\mathbf{u}}_1 \\ \widehat{\mathbf{u}}_2 \\ \widetilde{\mathbf{u}}_3 \\ \mathbf{u}_4 \\ \vdots \\ \overline{\mathbf{u}}_{n-4} \\ \widehat{\mathbf{u}}_{n-3} \\ \widetilde{\mathbf{u}}_{n-2} \\ \mathbf{u}_{n-1} \\ \mathbf{u}_n \end{bmatrix},$$

$$\mathscr{L} = \begin{bmatrix} \overline{g}_{\eta_{21}} & \overline{f}_{\eta_{21}} & 0_{3\times2} & 0_{3\times3} & 0_{3\times3} & \cdots & 0_{3\times3} & 0_{3\times2} & 0_{3\times2} & 0_{3\times3} & 0_{3\times3} \\ 0_{2\times3} & \widehat{g}_{h_{32}} & \widehat{f}_{h_{32}} & 0_{2\times3} & 0_{2\times3} & \cdots & 0_{2\times3} & 0_{2\times2} & 0_{2\times2} & 0_{2\times3} & 0_{2\times3} \\ 0_{2\times3} & 0_{2\times2} & \widetilde{g}_{h_{43}} & \widetilde{f}_{h_{43}} & 0_{2\times3} & \cdots & 0_{2\times3} & 0_{2\times2} & 0_{2\times2} & 0_{2\times3} & 0_{2\times3} \\ 0_{3\times3} & 0_{3\times2} & 0_{3\times2} & g_{\eta_{54}} & f_{\eta_{54}} & \cdots & 0_{3\times3} & 0_{3\times2} & 0_{3\times2} & 0_{3\times3} & 0_{3\times3} \\ \vdots & & & & \ddots & & & & & & \vdots \\ 0_{3\times3} & 0_{3\times2} & 0_{3\times2} & 0_{3\times3} & 0_{3\times3} & \cdots & \overline{g}_{\eta_{(n-3)(n-4)}} & \overline{f}_{\eta_{(n-3)(n-4)}} & 0_{3\times2} & 0_{3\times3} & 0_{3\times3} \\ 0_{2\times3} & 0_{2\times2} & 0_{2\times2} & 0_{2\times3} & 0_{2\times3} & \cdots & 0_{2\times3} & \widehat{g}_{h_{(n-2)(n-3)}} & \widehat{f}_{h_{(n-2)(n-3)}} & 0_{2\times3} & 0_{2\times3} \\ 0_{2\times3} & 0_{2\times2} & 0_{2\times2} & 0_{2\times3} & 0_{2\times3} & \cdots & 0_{2\times3} & 0_{2\times2} & \widetilde{g}_{h_{(n-1)(n-2)}} & \widetilde{f}_{h_{(n-1)(n-2)}} & 0_{2\times3} \\ 0_{3\times3} & 0_{3\times2} & 0_{3\times2} & 0_{3\times3} & 0_{3\times3} & \cdots & 0_{3\times3} & 0_{3\times2} & 0_{3\times2} & g_{\eta_{n(n-1)}} & f_{\eta_{n(n-1)}} \\ 0_{3\times3} & 0_{3\times2} & 0_{3\times2} & 0_{3\times3} & 0_{3\times3} & \cdots & 0_{3\times3} & 0_{3\times2} & 0_{3\times2} & 0_{3\times3} & R(\theta_n) \end{bmatrix}, \tag{31}$$

with $0_{a\times b}$ as an $a \times b$ zero matrix. Note that matrix $\mathscr{L}$ is still an upper triangular block matrix.

The linearizing feedback control law is given by

$$\mathbb{U} = \mathscr{L}^{-1}\mathbf{P}_d, \tag{32}$$

where

$$\mathbf{P}_d = \begin{bmatrix} \mathbf{p}_{21} \\ \widehat{\mathbf{p}}_{32} \\ \widetilde{\mathbf{p}}_{43} \\ \mathbf{p}_{54} \\ \vdots \\ \mathbf{p}_{(n-3)(n-4)} \\ \widehat{\mathbf{p}}_{(n-2)(n-3)} \\ \widetilde{\mathbf{p}}_{(n-1)(n-2)} \\ \mathbf{p}_{n(n-1)} \\ \mathbf{p}_n \end{bmatrix} \tag{33}$$

are the auxiliary controls defined previously.

Lemma 13. *Matrix $\mathscr{L}$ is always invertible for all $\alpha_{ji} \neq \pm\pi/2$ and $j \neq i$.*

Proof. Since matrix $\mathscr{L}$ is an upper triangular block matrix, hence, the determinant is given by the product of the determinants of the diagonal matrices. Specifically, for $n = 2$, the determinant of matrix $\mathscr{L}$ is defined as

$$\det(\mathscr{L}) = \frac{1}{d_{21}}, \tag{34}$$

while for $n \geq 3$, the determinant of matrix $\mathscr{L}$ is obtained as

$$\det(\mathscr{L}) = r\prod_{p,q}^{n} \frac{\cos\alpha_{q(q-1)}}{d_{p(p-1)}}, \tag{35}$$

where $p = 2, 5, 6, 9, 10\ldots, n$, $q = 3, 4, 7, 8, 11\ldots, n$, and

$$r = \begin{cases} -1, & \text{if } n = 3, 7, 11, \ldots \\ 1, & \text{otherwise.} \end{cases} \tag{36}$$

□

Proposition 14. *Consider system (29) in closed-loop with the control (32), then, the errors $e_{d_{ji}}$ and $e_{\alpha_{ji}}$ will converge to zero, i.e., $\lim_{t\longrightarrow\infty} e_{d_{ji}} = \lim_{t\longrightarrow\infty} e_{\alpha_{ji}} = 0$.*

Proof. Let us define the error coordinates as follows:

$$\mathbf{e} = \boldsymbol{\zeta} - \boldsymbol{\zeta}^*, \tag{37}$$

where $\boldsymbol{\zeta}^*$ is the desired vector of distances and orientations and is given as follows:

$$\boldsymbol{\zeta}^* = \begin{bmatrix} \overline{\boldsymbol{\eta}}^*_{21} \\ \widehat{\mathbf{h}}^*_{32} \\ \widetilde{\mathbf{h}}^*_{43} \\ \boldsymbol{\eta}^*_{54} \\ \vdots \\ \overline{\boldsymbol{\eta}}^*_{(n-3)(n-4)} \\ \widehat{\mathbf{h}}^*_{(n-2)(n-3)} \\ \widetilde{\mathbf{h}}^*_{(n-1)(n-2)} \\ \boldsymbol{\eta}^*_{n(n-1)} \\ \boldsymbol{\xi}^*_n \end{bmatrix}, \tag{38}$$

with $\overline{\boldsymbol{\eta}}^*_{ji} = \begin{bmatrix} d^*_{ji} & \alpha^*_{ji} & 0 \end{bmatrix}^\top$, $\widehat{\mathbf{h}}^*_{ji} = \begin{bmatrix} d^*_{ji} & \alpha^*_{ji} \end{bmatrix}^\top$, $\widetilde{\mathbf{h}}^*_{ji} = \begin{bmatrix} d^*_{ji} & \alpha^*_{ji} \end{bmatrix}^\top$, $\boldsymbol{\eta}^*_{ji} = \begin{bmatrix} d^*_{ji} & \alpha^*_{ji} & 0 \end{bmatrix}^\top$, and $\boldsymbol{\xi}^*_n = \begin{bmatrix} m_x & m_y & \theta_d \end{bmatrix}^\top$, for $j \neq i$, where m_x, m_y, and θ_d are the desired trajectory and orientation for the leader. The dynamics of the error coordinates are given by

$$\dot{\mathbf{e}} = \dot{\boldsymbol{\zeta}} - \dot{\boldsymbol{\zeta}}^*, \tag{39}$$

and substituting (29) with control (32) into (39), then one has

$$\dot{\mathbf{e}} = -K\mathbf{e}, \tag{40}$$

where

$$K = \operatorname{diag}\{K_{21}, K_{32}, K_{43}, K_{54}, K_{65}, \ldots, K_{n(n-1)}, K_n\}, \tag{41}$$

with $K_{21} = K_{54} = K_{65} = K_{n(n-1)} = \operatorname{diag}\{k_d, k_\alpha, k_\theta\}$, $K_{32} = K_{43} = \operatorname{diag}\{k_d, k_\alpha\}$, and $K_n = \operatorname{diag}\{k_{x_n}, k_{y_n}, k_{\theta_n}\}$. It becomes evident that if k_d, k_α, k_θ, k_{x_n}, k_{y_n}, and $k_{\theta_n} > 0$, hence, matrix K is Hurwitz, and the errors will converge to zero, *i.e.*, $\lim_{t\longrightarrow\infty} \mathbf{e} = 0$. □

Remark 15. The following results are interesting due to the fact that it is possible to show that the group of agents can emulate the kinematic behaviour of rigid bodies. As far as we know, this problem has not been addressed in the literature, considering the distance and the formation angle between a pair of robots.

4.6. Rigid Body Behaviour. It has been shown [39] that, when system (13) with control (15) and (16), reaches the steady state, then $\lim_{t\longrightarrow\infty} e_{d_{ji}} = \lim_{t\longrightarrow\infty} e_{\alpha_{ji}} = \lim_{t\longrightarrow\infty} e_{\theta_{ji}} = 0$ and the leader-follower scheme, composed by two omnidirectional mobile robots, will emulate the kinematic behaviour of a rigid body.

Based on the aforementioned, the following theorem states another contribution of this article.

Theorem 16. *Consider that, in system (13), the agents R_j and R_i can be either an omnidirectional or a differential-drive robot. Suppose that system (13) has reached the steady state and $d^*_{ji} =$*

$\bar{d}_{ji} \in \mathbb{R}_+$ *and* $\alpha^*_{ji} = 0$*; therefore, the leader-follower scheme will emulate the kinematic behaviour of a rigid body, the kinematic behaviour of a standard 1-trailer or the kinematic behaviour of the omnitrailer.*

The proof will be done constructively, taking into account the cases given in Sections 4.2, 4.3, and 4.4.

Proof (𝒰-𝒪 leader-follower scheme). Consider that system (19) with control (21) has reached the steady state, *i.e.*, $\lim_{t\longrightarrow\infty} e_{d_{ji}} = \lim_{t\longrightarrow\infty} e_{\alpha_{ji}} = \lim_{t\longrightarrow\infty} e_{\theta_{ji}} = 0$, then, substituting the control law (21) into the kinematic model (1), in steady state, one has

$$\begin{aligned}\dot{x}_i &= v_{x_j}\cos\theta_i - \bar{d}_{ji}w_j\sin\left(\alpha_{ji}-\theta_i\right),\\ \dot{y}_i &= v_{x_j}\sin\theta_i - \bar{d}_{ji}w_j\cos\left(\alpha_{ji}-\theta_i\right),\\ \dot{\theta}_i &= w_j.\end{aligned} \tag{42}$$

Due to $\lim_{t\longrightarrow\infty} e_{\theta_{ji}} = 0$, this means that $\lim_{t\longrightarrow\infty}\theta_i = \theta_j$, $\lim_{t\longrightarrow\infty}\alpha_{ji} = \alpha^*_{ji} = 0$, and the above expression is rewritten as

$$\begin{aligned}\dot{x}_i &= v_{x_j}\cos\theta_j + \bar{d}_{ji}w_j\sin\theta_j,\\ \dot{y}_i &= v_{x_j}\sin\theta_j - \bar{d}_{ji}w_j\cos\theta_j,\\ \dot{\theta}_i &= w_j.\end{aligned} \tag{43}$$

Note that, from (3), $\dot{x}_j = v_{x_j}\cos\theta_j$ and $\dot{y}_j = v_{x_j}\sin\theta_j$, then, one obtains

$$\dot{x}_i = \dot{x}_j + \bar{d}_{ji}w_j\sin\theta_j, \tag{44a}$$

$$\dot{y}_i = \dot{y}_j - \bar{d}_{ji}w_j\cos\theta_j, \tag{44b}$$

$$\dot{\theta}_i = w_j. \tag{44c}$$

Comparing these last expressions with respect to the rigid body motion equations (6a) and (6b), one can conclude that the follower will move such that the whole system will behave as a rigid body. □

Proof (𝒰-𝒰 leader-follower scheme). Consider that system (23) with control (25a) and (25b) has reached the steady state, *i.e.*, $\lim_{t\longrightarrow\infty} e_{d_{ji}} = \lim_{t\longrightarrow\infty} e_{\alpha_{ji}} = 0$; therefore, substituting the control law (25a) and (25b) into the kinematic model (3) and considering $d^*_{ji} = \bar{d}_{ji}$, in steady state, one has

$$\begin{aligned}\dot{x}_i &= \frac{v_{x_j}}{\cos\alpha^*_{ji}}\cos\theta_i\cos\left(\alpha^*_{ji}+e_{\theta_{ji}}\right),\\ \dot{y}_i &= \frac{v_{x_j}}{\cos\alpha^*_{ji}}\sin\theta_i\cos\left(\alpha^*_{ji}+e_{\theta_{ji}}\right),\\ \dot{\theta}_i &= \frac{v_{x_j}}{\bar{d}_{ji}\cos\alpha^*_{ji}}\sin e_{\theta_{ji}}.\end{aligned} \tag{45}$$

Then, letting $\alpha^*_{ji} = 0$ and $\theta_i = \theta_j - e_{\theta_{ji}}$, one obtains

$$\dot{x}_i = v_{x_j}\cos\left(\theta_j - e_{\theta_{ji}}\right)\cos e_{\theta_{ji}}, \tag{46a}$$

$$\dot{y}_i = v_{x_j}\sin\left(\theta_j - e_{\theta_{ji}}\right)\cos e_{\theta_{ji}}, \tag{46b}$$

$$\dot{\theta}_i = \frac{v_{x_j}}{\bar{d}_{ji}}\sin e_{\theta_{ji}}. \tag{46c}$$

Note that the linear velocity of agent R_i can be obtained from (46a) and (46b) as follows:

$$v_{x_i} = \sqrt{\dot{x}_i^2 + \dot{y}_i^2} = v_{x_j}\cos e_{\theta_{ji}}. \tag{47}$$

From Lemma 2 and comparing (47) with (8) and (46c) with (7d) one can note that they have the same structure. This means that the agent R_i will behave as a trailer and agent R_j as a tractor; hence, the whole system will behave as a standard 1−trailer. □

Proof (𝒪-𝒰 leader-follower scheme). Consider that system (23) with control (28) has reached the steady state, *i.e.*, $\lim_{t\longrightarrow\infty} e_{ji} = \lim_{t\longrightarrow\infty} e_{\alpha_{ji}} = 0$; therefore, substituting the control law (28) into the kinematic model of the follower (3) and considering that $\lim_{t\longrightarrow\infty} e_{d_{ji}} = \lim_{t\longrightarrow\infty} e_{\alpha_{ji}} = 0$, $d^*_{ji} = \bar{d}_{ji}$, in steady state, one has

$$\begin{aligned}\dot{x}_i &= \frac{\cos\theta_i}{\cos\alpha^*_{ji}}\left[v_{x_j}\cos\left(\alpha^*_{ji}+e_{\theta_{ji}}\right) - v_{y_j}\sin\left(\alpha^*_{ji}+e_{\theta_{ji}}\right)\right],\\ \dot{y}_i &= \frac{\sin\theta_i}{\cos\alpha^*_{ji}}\left[v_{x_j}\cos\left(\alpha^*_{ji}+e_{\theta_{ji}}\right) - v_{y_j}\sin\left(\alpha^*_{ji}+e_{\theta_{ji}}\right)\right],\\ \dot{\theta}_i &= \frac{1}{\bar{d}_{ji}\cos\alpha^*_{ji}}\left[v_{x_j}\sin e_{\theta_{ji}} + v_{y_j}\cos e_{\theta_{ji}}\right].\end{aligned} \tag{48}$$

Then, letting $\alpha^*_{ji} = 0$ and $\theta_i = \theta_j - e_{\theta_{ji}}$, one obtains

$$\dot{x}_i = \cos\left(\theta_j - e_{\theta_{ji}}\right)\left[v_{x_j}\cos e_{\theta_{ji}} - v_{y_j}\sin e_{\theta_{ji}}\right], \tag{49a}$$

$$\dot{y}_i = \sin\left(\theta_j - e_{\theta_{ji}}\right)\left[v_{x_j}\cos e_{\theta_{ji}} - v_{y_j}\sin e_{\theta_{ji}}\right], \tag{49b}$$

$$\dot{\theta}_i = \frac{1}{\bar{d}_{ji}}\left[v_{x_j}\sin e_{\theta_{ji}} + v_{y_j}\cos e_{\theta_{ji}}\right]. \tag{49c}$$

Note that the linear velocity of agent R_i can be obtained from (49a) and (49b) as follows:

$$v_{x_i} = \sqrt{\dot{x}_i^2 + \dot{y}_i^2} = v_{x_j}\cos e_{\theta_{ji}} - v_{y_j}\sin e_{\theta_{ji}}. \tag{50}$$

From Lemma 3 and comparing (50) with (9a) and (49c) with (9b), one can conclude that the leader-follower scheme will achieve the same kinematic behaviour of the omnitrailer given in Section 3.3. □

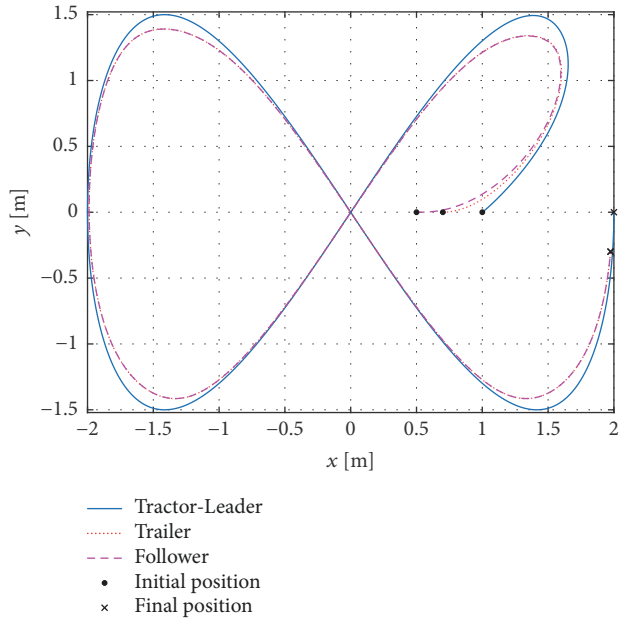

(a) Trajectory in the plane for a standard 1-trailer and the $\mathcal{U} - \mathcal{U}$ leader-follower scheme

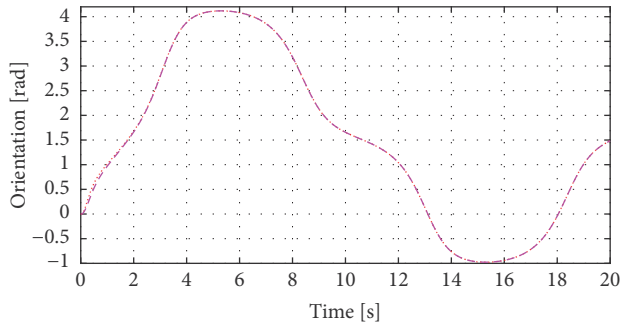

(b) Orientation angle of the trailer and the follower

FIGURE 3: Comparison behaviour between a standard 1-trailer and the $\mathcal{U} - \mathcal{U}$ leader-follower scheme.

5. Numerical Simulations

It is worth mentioning that the previous control strategies are defined between a pair of robots, where the follower robot is controlled with respect to a unique leader. If these behaviours are extended for the case of more than two robots, then it is possible to consider a graph topology with a directed tree-shaped configuration with a leader R_n following a desired trajectory. This topology can be constructed defining that, in each pair of robots R_i (follower) and R_j (leader), it is satisfied that $j > i$, $\forall i = 1, \ldots, n-1$, and $j = 1, \ldots, n$ with $j \neq i$.

For the first numerical simulation, Figure 3 displays a comparison between the kinematic behaviour of a standard 1−trailer, given by (7a), (7b), (7c), and (7d), and the $\mathcal{U} - \mathcal{U}$ leader-follower scheme, given by (23). The trailer receives commands of linear and angular velocities such that is following a Lemniscate of Gerono with parametrization $\boldsymbol{\xi}_d : \mathbb{R}_+ \longrightarrow \mathbb{R}^2$ given by

$$\boldsymbol{\xi}_d = \left[2\cos\left(\frac{\pi}{10}t\right) \;\; 1.5\sin\left(\frac{\pi}{5}t\right)\right]^\top. \tag{51}$$

The initial conditions for the standard 1−trailer are $[x_j(0) \;\; y_j(0) \;\; \theta_j(0) \;\; \theta_i(0)]^\top = [1 \;\; 0 \;\; 0 \;\; 0]^\top$ while for the follower are $\boldsymbol{\xi}_i(0) = [0.5 \;\; 0 \;\; 0]^\top$, with $\alpha^*_{ji} = 0$ rad, $d^*_{ji} = 0.3$ m and using the Matlab Simulink ode4 function solver [43]. Specifically, Figure 3(a) shows the trajectory in the plane for both, the standard 1−trailer, and the $\mathcal{U} - \mathcal{U}$ leader-follower scheme. It becomes evident that, in spite of the follower has different initial conditions with respect to the trailer, the follower has the same behaviour as the trailer; while Figure 3(b) shows the orientation for the trailer and the follower. Note that both orientation angles converge to the same value, allowing us to validate that the $\mathcal{U} - \mathcal{U}$ leader-follower scheme will behave as a standard 1−trailer.

In order to show the performance of the control law (32) and the different combinations of the leader-follower scheme, Figure 4 depicts a numerical simulation with $n = 13$. The leader robot $\mathcal{O}_{13}$ is controlled to follow a Lemmiscate of Gerono defined as

$$\boldsymbol{\xi}^*_{13} = \left[m_x, \;\; m_y, \;\; \arctan\left(\frac{\dot{m}_y}{\dot{m}_x}\right)\right]^\top, \tag{52}$$

with $m_x = 4\cos((\pi/10)t)$, $m_y = 3\sin((\pi/5)t)$, and $K_{13} = \text{diag}\{1, 1, 3\}$. Since the agents are under the leader-follower topology, then, the desired distance and the formation angle are the same for all the pair of robots, *i.e.*, $d^*_{ji} = 0.2$ m and $\alpha^*_{ji} = 0$ rad, while the control parameters are $K_{21} = K_{54} = K_{65} = K_{98} = K_{109} = K_{1312} = \text{diag}\{2, 2, 3\}$ and $K_{32} = K_{43} = K_{76} = K_{87} = K_{98} = K_{1110} = K_{1211} = \text{diag}\{2, 2\}$. The initial conditions for the robots are

$$\boldsymbol{\xi}_1(0) = [0.89 \;\; 0.085 \;\; 0]^\top,$$
$$\boldsymbol{\xi}_2(0) = [1.14 \;\; -0.0905 \;\; 0]^\top,$$
$$\boldsymbol{\xi}_3(0) = [1.33 \;\; -0.288 \;\; 0]^\top,$$
$$\boldsymbol{\xi}_4(0) = [1.52 \;\; -0.104 \;\; 0]^\top,$$
$$\boldsymbol{\xi}_5(0) = [1.74 \;\; -0.186 \;\; 0]^\top,$$
$$\boldsymbol{\xi}_6(0) = [1.89 \;\; -0.117 \;\; 0]^\top,$$
$$\boldsymbol{\xi}_7(0) = [2.02 \;\; -0.153 \;\; 0]^\top,$$
$$\boldsymbol{\xi}_8(0) = [2.139 \;\; -0.112 \;\; 0]^\top,$$

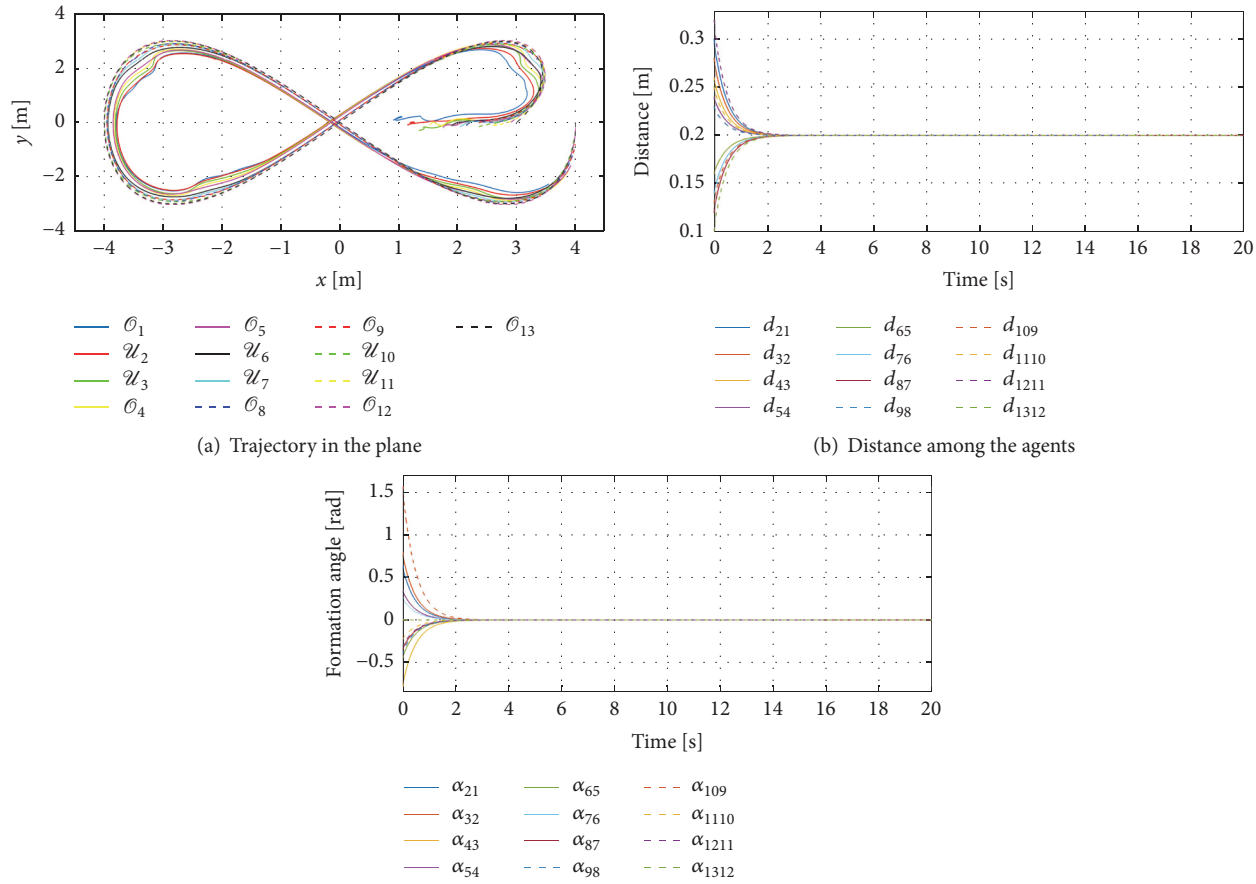

(a) Trajectory in the plane

(b) Distance among the agents

(c) Formation angles

FIGURE 4: Simulation with $n = 13$ combining the four different leader-follower schemes.

$$\begin{aligned}
\boldsymbol{\xi}_9(0) &= \begin{bmatrix} 2.35 & -0.024 & 0 \end{bmatrix}^\top, \\
\boldsymbol{\xi}_{10}(0) &= \begin{bmatrix} 2.352 & 0.154 & 0 \end{bmatrix}^\top, \\
\boldsymbol{\xi}_{11}(0) &= \begin{bmatrix} 2.59 & -0.098 & 0 \end{bmatrix}^\top, \\
\boldsymbol{\xi}_{12}(0) &= \begin{bmatrix} 2.9 & 0 & 0 \end{bmatrix}^\top, \\
\boldsymbol{\xi}_{13}(0) &= \begin{bmatrix} 3 & 0 & 0 \end{bmatrix}^\top.
\end{aligned} \tag{53}$$

Particularly, Figure 4(a) illustrates the trajectory in the plane of all the robots. In this sense, the pairs of robots $(\mathcal{O}_5, \mathcal{O}_4)$, $(\mathcal{O}_9, \mathcal{O}_8)$, and $(\mathcal{O}_{13}, \mathcal{O}_{12})$ are under the $\mathcal{O} - \mathcal{O}$ scheme while the pairs of robots $(\mathcal{U}_2, \mathcal{O}_1)$, $(\mathcal{U}_6, \mathcal{O}_5)$, and $(\mathcal{U}_{10}, \mathcal{O}_9)$ are under the $\mathcal{U} - \mathcal{O}$ scheme. In both cases, the agents achieve the rigid body behaviour. For the $\mathcal{U} - \mathcal{U}$ scheme, integrated by the pairs $(\mathcal{U}_3, \mathcal{U}_2)$, $(\mathcal{U}_7, \mathcal{U}_6)$, and $(\mathcal{U}_{11}, \mathcal{U}_{10})$, it achieves the behaviour of the standard 1–trailer. The omnitrailer behaviour appears in the pairs $(\mathcal{O}_4, \mathcal{U}_3)$, $(\mathcal{O}_8, \mathcal{U}_7)$, and $(\mathcal{O}_{12}, \mathcal{U}_{11})$ with the $\mathcal{O} - \mathcal{U}$ scheme. Note that, in all the cases, the pairs of robots satisfy $j > i$. On the other hand, Figure 4(b) depicts the distance among the robots, where it becomes evident that each pair of agents converges to the desired distance $d_{ji}^* = 0.2$ m. Finally, Figure 4(c) displays the formation angles of each pair of agents, which converge to the desired formation angle $\alpha_{ji}^* = 0$ rad.

6. Experimental Work

The approach is tested using the four mobile robots with four mecanum wheels like the ones shown in Figure 5(a). The robots are actuated by servomotors Dynamixel® AX − 12W and controlled by a microcontroller NXP® model *LPC*1768 with Bluetooth communication to a PC computer using the module *HC*−05. In a first step, the position and orientation of the robots are measured by a Vicon® motion capture system composed by 6 cameras model Bonita® (Figure 5(b)). The motion capture measures within an available workspace area of 3 m by 0.7 m. Note in Figure 5(a) that the reflective markers were placed on the top of the robots in order to be identified by the Vicon® system. The control algorithm runs at 117 ms rate with a resolution of ±0.5 mm.

According to Figure 6, the velocities of each wheel can be calculated by

$$\begin{bmatrix} \omega_{i_1} \\ \omega_{i_2} \\ \omega_{i_3} \\ \omega_{i_4} \end{bmatrix} = \frac{1}{r} \begin{bmatrix} 1 & -1 & -(L+l) \\ 1 & 1 & (L+l) \\ 1 & 1 & (L+l) \\ 1 & -1 & -(L+l) \end{bmatrix} \begin{bmatrix} v_{x_i} \\ v_{y_i} \\ \omega_i \end{bmatrix}, \tag{54}$$

where $L = 0.1$ m, $l = 0.05$ m, and $r = 0.0275$ m. Note that (54) can be adequate according to the number of wheels of

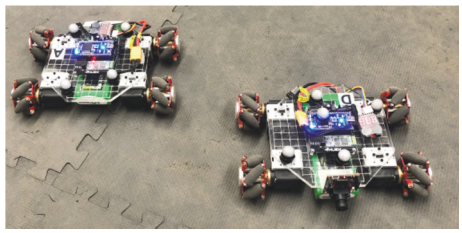

(a) Omnidirectional wheeled mobile robots

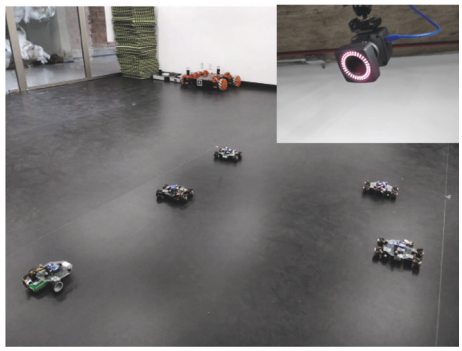

(b) Experimental setup

FIGURE 5: Experimental setup composed by omnidirectional and differential-drive mobile robots and six Vicon cameras.

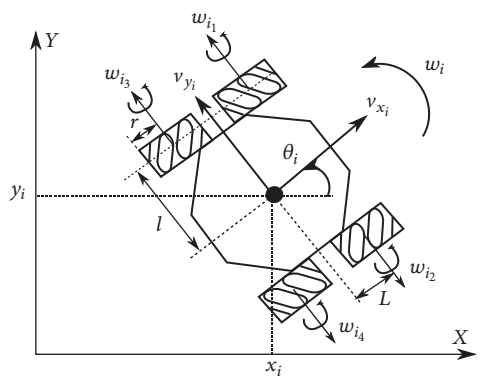

FIGURE 6: Omnidirectional wheeled mobile robot.

the robot, for example, for the three omnidirectional wheeled mobile robot.

Figures 7, 8, and 9 show an experiment of the combined four control laws presented in the Section 4. The leader robot is $\mathcal{O}_4$ (omnidirectional robot in black color). The pair $(\mathcal{O}_4, \mathcal{O}_3)$ implements the control $\mathcal{O} - \mathcal{O}$ scheme, achieving a rigid body behaviour. The pair $(\mathcal{O}_4, \mathcal{U}_2)$ enables the control law $\mathcal{O} - \mathcal{U}$ scheme, obtaining an omnitrailer behaviour. Finally, the pair $(\mathcal{U}_2, \mathcal{O}_1)$ implements the control law $\mathcal{U} - \mathcal{O}$ scheme performing another rigid body behaviour. The desired distance and heading angles are given by $d_{43}^* = d_{42}^* = d_{21}^* = 0.3$ m and $\alpha_{43}^* = -\pi/2$ rad, $\alpha_{42}^* = 0$ rad, and $\alpha_{21}^* = \pi/2$. The control parameters are $K_{ji} = \text{diag}\{6, 6, 2\}$ for the pairs $(\mathcal{O}_4, \mathcal{O}_3)$ and $(\mathcal{U}_2, \mathcal{O}_1)$ and $K_{42} = \text{diag}\{5, 1\}$ for the pair $(\mathcal{O}_4, \mathcal{U}_2)$. The initial conditions of the robots are given by

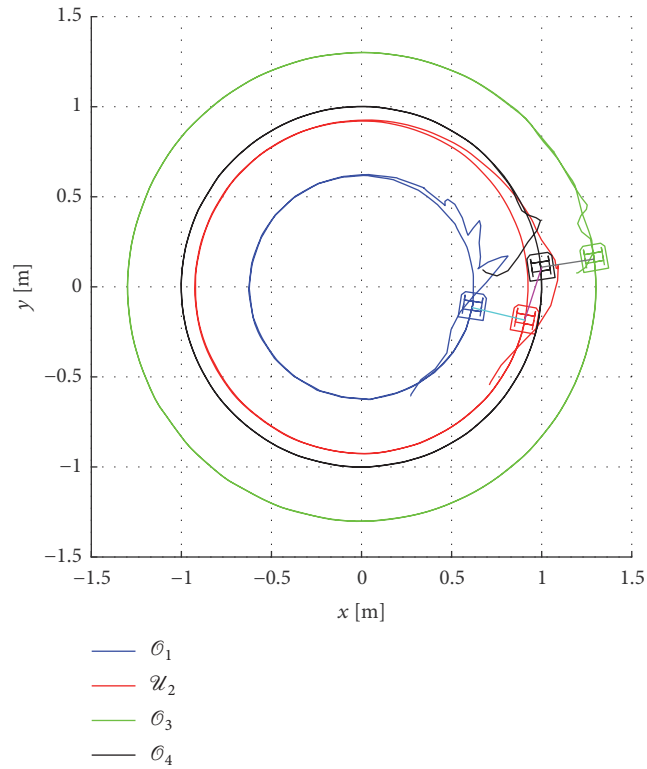

FIGURE 7: Trajectories in the plane with $n = 4$ agents. The agent $\mathcal{U}_2$ is an omnidirectional robot with lateral velocity $v_{y_2} = 0$ allowing him to act as a differential-drive robot.

$$\begin{aligned}
\boldsymbol{\xi}_1(0) &= \begin{bmatrix} 0.6163 & -0.10531 & -12.41 \end{bmatrix}^\top \\
\boldsymbol{\xi}_2(0) &= \begin{bmatrix} 0.9072 & -0.17935 & -12.38 \end{bmatrix}^\top, \\
\boldsymbol{\xi}_3(0) &= \begin{bmatrix} 1.2902 & -0.16269 & -1.274 \end{bmatrix}^\top, \\
\boldsymbol{\xi}_4(0) &= \begin{bmatrix} 0.9943 & -0.11272 & -12.71 \end{bmatrix}^\top,
\end{aligned} \tag{55}$$

in meters and radians, respectively. The leader robot is controlled to follow a circled-shape trajectory with radius equal to 1 m centered on the origin and oriented to the velocity vector of the trajectory; *i.e.,* the desired values for the leader are given by

$$\boldsymbol{\xi}_4^* = \left[m_x, \; m_y, \; \arctan\left(\frac{\dot{m}_y}{\dot{m}_x}\right) - \frac{\pi}{2} \right]^\top, \tag{56}$$

where $m_x = \sin((2\pi/25)t)$ and $m_y = \cos((2\pi/25)t)$. Thus, the control law for the leader robot is established as $\mathbf{u}_4 = R^{-1}(\theta_4)[\dot{\boldsymbol{\xi}}_4^* - k_4(\boldsymbol{\xi}_4 - \boldsymbol{\xi}_4^*)]$, with $k_4 = \text{diag}\{6, 6, 2.5\}$.

The trajectories of the robots are shown in Figure 7. The colors of the links between robots in Figure 7 identify the type of control law that it is being used, *i.e.,* gray color for $\mathcal{O} - \mathcal{O}$ scheme, magenta color for $\mathcal{O} - \mathcal{U}$ scheme, and cyan color for $\mathcal{U} - \mathcal{O}$ scheme. Note that, in all cases, it is satisfied that $j > i$. Furthermore, in this experiment, the agent $\mathcal{U}_2$ is an omnidirectional mobile robot with $v_{y_2} = 0$ obtaining the behaviour of a differential-drive robot. It is important to point out that, from a global point of view, a leader-follower

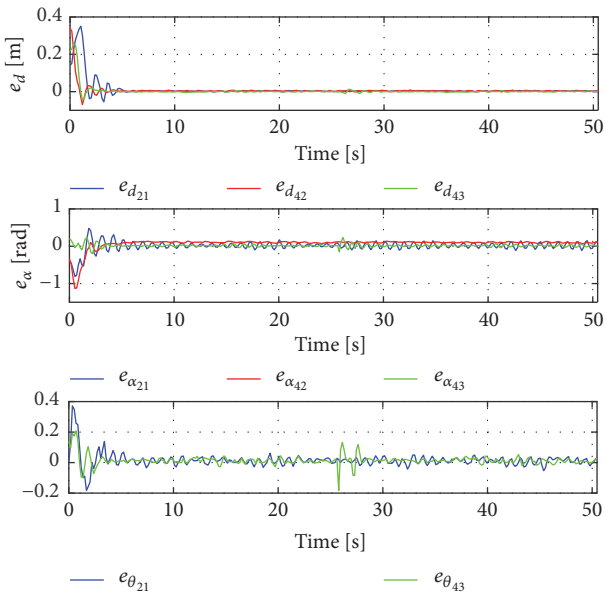

FIGURE 8: Distance error, formation angle error, and orientation error.

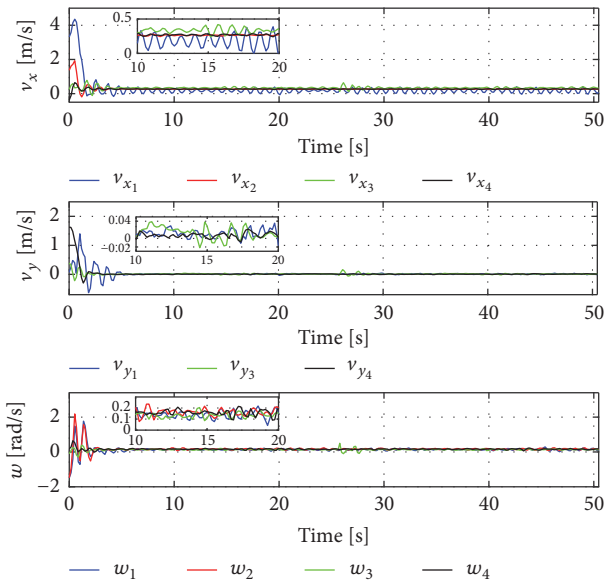

FIGURE 9: Control inputs for the mobile robots.

setup with subsets or platoons of robots is achieved. This kind of system can be applied in collaborative transportation tasks where the platoons of robots load together a big workpiece and all the platoons are formed in a convoy-like configuration.

From Figure 8, it becomes clear that each follower converges to the desired distance and the desired formation angle. Finally, Figure 9 depicts the control inputs for each robot. Noise effects in the trajectories appear due to the nonmodelled friction of the wheels on the floor, sensor measurements, and actuator errors, among others.

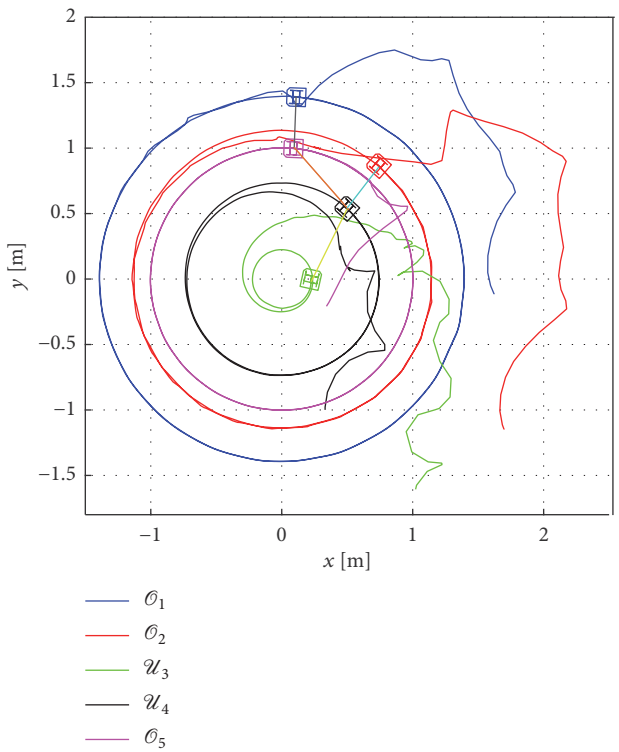

FIGURE 10: Trajectories in the plane with $n = 5$ agents. The agent $\mathcal{U}_4$ is an omnidirectional robot with lateral velocity $v_{y_4} = 0$ allowing him to act as a differential-drive robot while $\mathcal{U}_3$ is a differential-drive robot.

A second experiment with $n = 5$ agents is displayed in Figures 10, 11, and 12. In this case, the group of agents is composed by a differential-drive mobile robot and four omnidirectional robots, where one of them acts as a differential-drive robot. The initial conditions of the robots are given by

$$\begin{aligned}
\boldsymbol{\xi}_1(0) &= \begin{bmatrix} 1.62 & -0.11 & 2.68 \end{bmatrix}^\top, \\
\boldsymbol{\xi}_2(0) &= \begin{bmatrix} 1.69 & -1.14 & 2.21 \end{bmatrix}^\top, \\
\boldsymbol{\xi}_3(0) &= \begin{bmatrix} 1.02 & -1.6 & 1.16 \end{bmatrix}^\top, \\
\boldsymbol{\xi}_4(0) &= \begin{bmatrix} 0.33 & -0.99 & -0.2 \end{bmatrix}^\top, \\
\boldsymbol{\xi}_5(0) &= \begin{bmatrix} 0.34 & -0.2 & 0.93 \end{bmatrix}^\top,
\end{aligned} \tag{57}$$

in meters and radians, respectively. The leader robot is controlled to follow the same circled-shape trajectory of the previous experiment. The trajectories in the plane are depicted in Figure 10. The leader robot is $\mathcal{O}_5$ (omnidirectional robot in magenta color). The pair $(\mathcal{O}_5, \mathcal{U}_4)$ implements the control $\mathcal{O} - \mathcal{U}$ scheme, achieving the omnitrailer behaviour, illustrated by an orange line. The pair $(\mathcal{O}_5, \mathcal{O}_1)$ enables the control law $\mathcal{O} - \mathcal{O}$ scheme while the pair $(\mathcal{U}_4, \mathcal{O}_2)$ enables the control law $\mathcal{U} - \mathcal{O}$ scheme, obtaining, in both cases, a rigid body behaviour, depicted by a gray and cyan line, respectively. Finally, the pair $(\mathcal{U}_4, \mathcal{U}_3)$ implements the control law $\mathcal{U} - \mathcal{U}$ scheme performing the standard 1– trailer behaviour, represented by the yellow line.

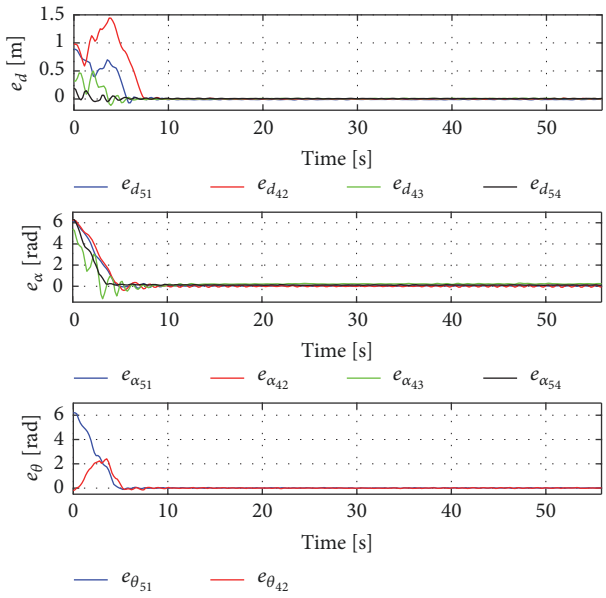

Figure 11: Distance error, formation angle error, and orientation error.

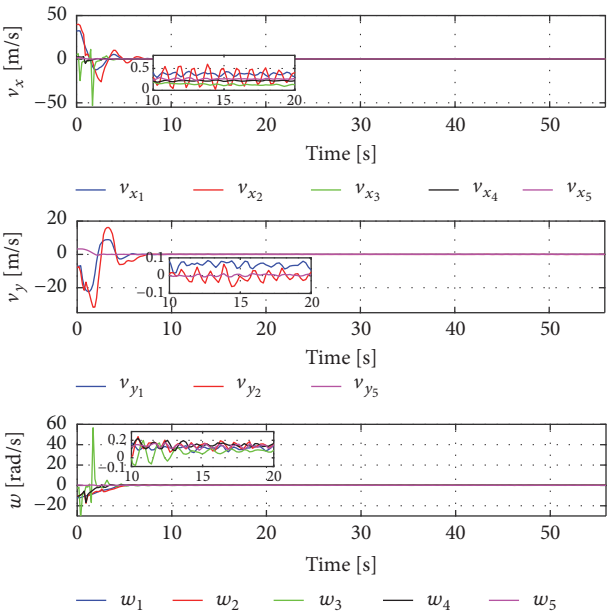

Figure 12: Control inputs for the mobile robots.

The desired distance and heading angles are given by $d_{51}^* = d_{42}^* = 0.4$ m, $d_{54}^* = d_{43}^* = 0.6$ m, $\alpha_{51}^* = \alpha_{42}^* = \pi/2$ rad, and $\alpha_{54}^* = \alpha_{43}^* = 0$ rad. The control parameters are the same as in the previous experiment *i.e.*, $K_{ji} = \text{diag}\{6, 6, 2\}$ for the pairs $(\mathcal{O}_5, \mathcal{O}_1)$ and $(\mathcal{U}_4, \mathcal{O}_2)$ and $K_{54} = K_{43} = \text{diag}\{5, 1\}$ for the pairs $(\mathcal{O}_5, \mathcal{U}_4)$ and $(\mathcal{O}_4, \mathcal{U}_3)$.

The distance error, the formation angle error, and the orientation error are displayed in Figure 11. Note that each follower converges to the desired distance and the desired formation angle. On the other hand, the control inputs for each mobile robot are shown in Figure 12.

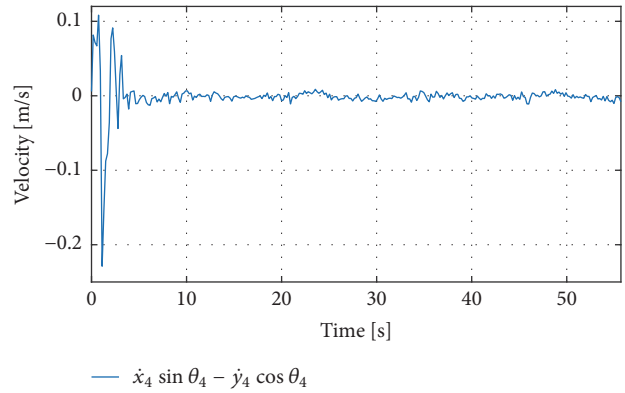

Figure 13: Nonholonomic restriction for the agent $\mathcal{U}_4$ which is an omnidirectional robot acting as a differential-drive robot.

Finally, in order to show that agent $\mathcal{U}_4$ behaves as a differential-drive robot, Figure 13 illustrates the nonholonomic restriction of this agent. This signal was obtained by applying a numerical method to calculate the derivative of x_4 and y_4. Note that, in steady state, the nonholonomic restriction converges to a band with magnitude given in terms of the measurement error. This means that the nonholonomic restriction is satisfied by the agent $\mathcal{U}_4$.

7. Conclusions

This work extends the leader-follower behaviours of a combined set of several kinematic models of omnidirectional and differential-drive robots. This kind of robots becomes actually in the most common wheeled vehicles used in the industry and service tasks. By the combination of these models, four basic leader-follower control laws are designed using the measurements of distance and the heading angle with respect to a leader, avoiding the use of a global reference framework. It is proved that these control laws generate, in the settling time, some mechanical structures related to rigid body, the standard 1-trailer, and a new structure called omnitrailer. Extending this local behaviour to the case of multiple groups of agents, a directed tree-shaped topology can be constructed, where the leader robot is the unique root node.

It is shown by numerical simulations and real-time experiments that the combination of the leader-follower setups can generate formation tracking, useful for object transportation or other collaborative tasks, like n-trailer and convoy behaviours of rigid platoons of robots. This complex behaviour becomes a more decentralized approach than the global referenced strategies like virtual structures or cluster space specifications. As future work, the formation topologies will be extended for other directed and undirected graphs and the local sensors will be implemented in the robots to measure the distances and the heading angles.

Data Availability

No data were used to support this study.

Conflicts of Interest

The authors declare that they have no conflicts of interest.

Acknowledgments

This work was supported by Universidad Iberoamericana, CONACyT Mexico, Universidad Católica del Uruguay, and ANII Uruguay.

Supplementary Materials

Supplemental material has included a short video of the second experiment with 5 agents. In this case, the leader robot is an $\mathcal{O}_5$ (omnidirectional robot). The pair $(\mathcal{O}_5, \mathcal{U}_4)$ implements the control $\mathcal{O} - \mathcal{U}$ scheme, achieving the omnitrailer behaviour. The pair $(\mathcal{O}_5, \mathcal{O}_1)$ enables the control law $\mathcal{O} - \mathcal{O}$ scheme while the pair $(\mathcal{U}_4, \mathcal{O}_2)$ enables the control law $\mathcal{U} - \mathcal{O}$ scheme, obtaining, in both cases, a rigid body behaviour. Finally, the pair $(\mathcal{U}_4, \mathcal{U}_3)$ implements the control law $\mathcal{U} - \mathcal{U}$ scheme performing the standard 1− trailer behaviour. *(Supplementary Materials)*

References

[1] W. Ren and R. Beard, *Distributed Consensus in Multi-vehicle Cooperative Control*, Springer, London, UK, 2008.

[2] H. Oh, A. Ramezan Shirazi, C. Sun, and Y. Jin, "Bio-inspired self-organising multi-robot pattern formation: A review," *Robotics and Autonomous Systems*, vol. 91, pp. 83–100, 2017.

[3] K.-K. Oh, M.-C. Park, and H.-S. Ahn, "A survey of multi-agent formation control," *Automatica*, vol. 53, pp. 424–440, 2015.

[4] A. Lopez-Gonzalez, E. D. Ferreira, E. G. Hernandez-Martinez, J. J. Flores-Godoy, G. Fernandez-Anaya, and P. Paniagua-Contro, "Multi-robot formation control using distance and orientation," *Advanced Robotics*, vol. 30, no. 14, pp. 901–913, 2016.

[5] Y. Zheng, Y. Zhu, and L. Wang, "Consensus of heterogeneous multi-agent systems," *IET Control Theory & Applications*, vol. 5, no. 16, pp. 1881–1888, 2011.

[6] J. P. Desai, J. P. Ostrowski, and V. Kumar, "Modeling and control of formations of nonholonomic mobile robots," *IEEE Transactions on Robotics and Automation*, vol. 17, no. 6, pp. 905–908, 2001.

[7] N. Soltani, A. Shahmansoorian, and M. A. Khosravi, "Robust distance-angle leader-follower formation control of nonholonomic mobile robots," in *Proceedings of 2014 Second RSI/ISM International Conference on Robotics and Mechatronics (ICRoM)*, pp. 024–028, October 2014.

[8] S. Kang, M. Park, B. Lee, and H. Ahn, "Distance-based formation control with a single moving leader," in *Proceedings of the American Control Conference*, vol. 1, pp. 305–310, 2014.

[9] M. A. Dehghani and M. B. Menhaj, "Communication free leader-follower formation control of unmanned aircraft systems," *Robotics and Autonomous Systems*, vol. 80, pp. 69–75, 2016.

[10] H. Garcia De Marina, B. Jayawardhana, and M. Cao, "Distributed rotational and translational maneuvering of rigid formations and their applications," *IEEE Transactions on Robotics*, vol. 32, no. 3, pp. 684–697, 2016.

[11] O. Rozenheck, S. Zhao, and D. Zelazo, "A proportional-integral controller for distance-based formation tracking," in *Proceedings the 2015 European Control Conference (ECC)*, pp. 1693–1698, 2015.

[12] G. Antonelli, F. Arrichiello, F. Caccavale, and A. Marino, "Decentralized time-varying formation control for multi-robot systems," *International Journal of Robotics Research*, vol. 33, no. 7, pp. 1029–1043, 2014.

[13] B. D. O. Anderson, Z. Sun, T. Sugie, S. I. Azuma, and K. Sakurama, "Formation shape control with distance and area constraints," *IFAC Journal of Systems and Control*, 2017.

[14] M. Basiri, A. N. Bishop, and P. Jensfelt, "Distributed control of triangular formations with angle-only constraints," *Systems & Control Letters*, vol. 59, no. 2, pp. 147–154, 2010.

[15] H. Xiao, Z. Li, and C. L. Philip Chen, "Formation control of leader-follower mobile robots systems using model predictive control based on neural-dynamic optimization," *IEEE Transactions on Industrial Electronics*, vol. 63, no. 9, pp. 5752–5762, 2016.

[16] Y. Shang and Y. Ye, "Leader-follower fixed-time group consensus control of multiagent systems under directed topology," *Complexity*, vol. 2017, Article ID 3465076, 9 pages, 2017.

[17] W. Ren and N. Sorensen, "Distributed coordination architecture for multi-robot formation control," *Robotics and Autonomous Systems*, vol. 56, no. 4, pp. 324–333, 2008.

[18] A. Morales and H. Nijmeijer, "Merging strategy for vehicles by applying cooperative tracking control," *IEEE Transactions on Intelligent Transportation Systems*, vol. 17, no. 12, pp. 3423–3433, 2016.

[19] G. Arechavaleta, A. Morales-Diaz, H. M. Perez-Villeda, and M. Castelan, "Hierarchical task-based control of multirobot systems with terminal attractors," *IEEE Transactions on Control Systems Technology*, vol. 25, no. 1, pp. 334–341, 2017.

[20] C. Canudas, B. Siciliano, and G. Bastin, *Theory of Robot Control*, Springer, London, UK, 1996.

[21] M. A. Neumann and C. A. Kitts, "A hybrid multirobot control architecture for object transport," *IEEE/ASME Transactions on Mechatronics*, vol. 21, no. 6, pp. 2983–2988, 2016.

[22] J. T. Cook, L. E. Ray, and J. H. Lever, "Dynamics modeling and robotic-assist, leader-follower control of tractor convoys," *Journal of Terramechanics*, vol. 75, pp. 57–72, 2018.

[23] E. H. C. Harik, F. Gu, F. Guinand et al., "Uav-ugv cooperation for objects transportation in an industrial area," in *Proceedings of the 2015 IEEE International Conference on Industrial Technology (ICIT)*, pp. 547–552, 2015.

[24] M. A. Dehghani, M. B. Menhaj, and M. Azimi, "Leader-follower formation control using an onboard leader tracker," in *Proceedings of the 4th International Conference on Control, Instrumentation, and Automation, ICCIA 2016*, pp. 99–104, Iran, January 2016.

[25] D. Guo, H. Wang, W. Chen, M. Liu, Z. Xia, and K. K. Leang, "A unified leader-follower scheme for mobile robots with uncalibrated on-board camera," in *Proceedings of the 2017 IEEE International Conference on Robotics and Automation, ICRA 2017*, pp. 3792–3797, Singapore, May 2017.

[26] B. Fidan, V. Gazi, S. Zhai, N. Cen, and E. Karatas, "Single-view distance-estimation-based formation control of robotic swarms," *IEEE Transactions on Industrial Electronics*, vol. 60, no. 12, pp. 5781–5791, 2013.

[27] D. Panagou and V. Kumar, "Cooperative visibility maintenance for leader-follower formations in obstacle environments," *IEEE Transactions on Robotics*, vol. 30, no. 4, pp. 831–844, Aug 2014.

[28] F. Li, Y. Ding, M. Zhou, K. Hao, and L. Chen, "An affection-based dynamic leader selection model for formation control in multirobot systems," *IEEE Transactions on Systems, Man, and Cybernetics: Systems*, vol. 47, no. 7, pp. 1217–1228, 2017.

[29] R. Kobayashi, M. Suzuki, and K. Nakano, "Leader-following formation navigation with virtual trajectories for dynamic multi-agents," *IFAC Proceedings Volumes*, vol. 46, no. 21, pp. 773–779, 2013, 7th IFAC Symposium on Advances in Automotive Control.

[30] H. Rezaee and F. Abdollahi, "A decentralized cooperative control scheme with obstacle avoidance for a team of mobile robots," *IEEE Transactions on Industrial Electronics*, vol. 61, no. 1, pp. 347–354, 2014.

[31] J.-W. Kwon and D. Chwa, "Hierarchical formation control based on a vector field method for wheeled mobile Robots," *IEEE Transactions on Robotics*, vol. 28, no. 6, pp. 1335–1345, 2012.

[32] D. Zhou, Z. Wang, and M. Schwager, "Agile coordination and assistive collision avoidance for quadrotor swarms using virtual structures," *IEEE Transactions on Robotics*, vol. 34, no. 4, pp. 916–923, 2018.

[33] L. Dong, Y. Chen, and X. Qu, "Formation control strategy for nonholonomic intelligent vehicles based on virtual structure and consensus approach," in *Proceedings of the Green Intelligent Transportation System and Safety, GITSS 2015*, pp. 415–424, Procedia Engineering, China, 2016.

[34] W. Ren and R. W. Beard, "Formation feedback control for multiple spacecraft via virtual structures," *IEE Proceedings Control Theory and Applications*, vol. 151, no. 3, pp. 357–368, 2004.

[35] X. Cai and M. D. Queiroz, "Adaptive rigidity-based formation control for multirobotic vehicles with dynamics," *IEEE Transactions on Control Systems Technology*, vol. 23, no. 1, pp. 389–396, 2015.

[36] A. D. Dang and J. Horn, "Formation control of autonomous robots following desired formation during tracking a moving target," in *Proceedings of the 2nd IEEE International Conference on Cybernetics, CYBCONF 2015*, pp. 160–165, Poland, June 2015.

[37] C. Kitts and I. Mas, "Cluster space specification and control of mobile multirobot systems," *IEEE/ASME Transactions on Mechatronics*, vol. 14, no. 2, pp. 207–218, 2009.

[38] I. Mas and C. A. Kitts, "Dynamic control of mobile multirobot systems: the cluster space formulation," *IEEE Access*, vol. 2, pp. 558–570, 2014.

[39] J. González-Sierra, E. Hernández-Martínez, E. D. Ferreira-Vazquez et al., "Leader-follower control strategy with rigid body behavior," in *Proceedings of the 12th IFAC Symposium on Robot Control*, vol. 51, Budapest, Hungary, August 2018.

[40] P. Rouchon, M. Fliessand, J. Lévine, and P. Martin, "Flatness and motion planning: the car with n trailers," in *Proceedings of the European Control Conference*, Groningen, Netherlands, 1993.

[41] R. Orosco-Guerrero, E. Aranda-Bricaire, and M. Velasco-Villa, "Modeling and dynamic feedback linearization of a multi-steered n-trailer," in *Proceedings of the 15th Triennial IFAC World Congress*, Barcelona, Spain, 2002.

[42] L. Bushnell, D. Tilbury, and S. Sastry, "Steering three-input chained form nonholonomic systems using sinusoids: the fire truck example," in *Proceedings of the European Control Conference*, pp. 1432–1437, Groningen, Netherlands, 1993.

[43] The MathWorks Inc., *Simulink User's Guide*, 2018.